Monthly Notices
of the
ROYAL ASTRONOMICAL SOCIETY

Mon. Not. R. Astron. Soc. **417,** 555–566 (2011) doi:10.1111/j.1365-2966.2011.19297.x

Flares and proper motions of ground-state OH masers in W75N

Vincent L. Fish,[1⋆] Malcolm Gray,[2⋆] W. M. Goss[3⋆] and A. M. S. Richards[2⋆]

[1]*MIT Haystack Observatory, Route 40, Westford, MA 01886, USA*
[2]*Jodrell Bank Centre for Astrophysics, The Alan Turing Building, School of Physics and Astronomy, The University of Manchester, Oxford Road, Manchester M13 9PL*
[3]*National Radio Astronomy Observatory, 1003 Lopezville Road, PO Box O, Socorro, NM 87801, USA*

Accepted 2011 June 20. Received 2011 June 20; in original form 2011 April 26

ABSTRACT

The star-forming region W75N hosts bright OH masers that are observed to be variable. We present observations taken in 2008 of the ground-state OH maser transitions with the Very Long Baseline Array and the Multi-Element Radio-Linked Interferometer Network and with the Nançay Radio Telescope in 2011. Several of the masers in W75N were observed to be flaring, with the brightest 1720-MHz maser in excess of 400 Jy. The 1720-MHz masers appear to be associated with the continuum source VLA 1, unlike the bright flaring 1665- and 1667-MHz masers, which are associated with VLA 2. The 1720-MHz masers are located in an outflow traced by water masers and are indicative of very dense molecular material near the H II region. The magnetic field strengths are larger in the 1720-MHz maser region than in most regions hosting only main-line OH masers. The density falls off along the outflow, and the order of appearance of different transitions of OH masers is consistent with theoretical models. The 1665- and 1667-MHz VLBA data are compared against previous epochs over a time baseline of over 7 years. The median maser motion is 3.5 km s^{-1} with a scatter that is comparable to thermal turbulence. The general pattern of maser proper motions observed in the 1665- and 1667-MHz transitions is consistent with previous observations.

Key words: magnetic fields – masers – stars: formation – ISM: individual objects: W75N – ISM: kinematics and dynamics – radio lines: ISM.

1 INTRODUCTION

The Galactic star-forming region W75N, located at a distance of 1.3 kpc (Rygl et al. 2010), is known to host bright OH masers with significant variability. Observations of the 1665-MHz masers have detected flares above 1000 Jy, making W75N temporarily the brightest OH maser source in the sky (Alakoz et al. 2005; Slysh, Alakoz & Migenes 2010). The brightest masers, found near the continuum source VLA 2 (as defined in Torrelles et al. 1997), also exhibit the greatest variability. Many observations have focused exclusively on the main-line 1665- and 1667-MHz transitions, which are distributed throughout W75N (Fish et al. 2005), rather than on the satellite-line 1720-MHz masers, which are concentrated in one area and have previously been observed to have a peak flux of only a few Jy (Hutawarakorn, Cohen & Brebner 2002).

Owing to their intensity and compactness, masers are often used as kinematic tracers of their environment, with motions usually being deduced from multi-epoch very long baseline interferometric (VLBI) observations. Norris & Booth (1981), Migenes, Cohen & Brebner (1992) and Bloemhof, Reid & Moran (1992) were among the first to measure proper motions of OH masers in star-forming regions. Due to the demanding nature of VLBI observations, proper motion measurements of ground-state OH masers have rarely been made over more than two epochs (e.g. Wright, Gray & Diamond 2004; Fish & Reid 2007a,b). In most sources, these studies find large-scale ordered motions of the OH masers, although individual motion vectors appear to have a large random component. One disadvantage of using a two-epoch set of observations is the inability to determine what portion of an apparent maser motion is real and what portion is due to random errors, although the existence of large-scale ordered motions strongly supports the interpretation of apparent motions as real, if noisy, indicators of actual maser motions. However, a recent multi-epoch study of the ground-state OH masers in W75N by Slysh et al. (2010) suggests that the random errors dominate, preventing estimation of the actual maser motions in most cases.

In this manuscript, we report on two epochs of observations of ground-state OH transitions with the Very Long Baseline Array (VLBA) and one epoch of observations of the 1720-MHz

⋆E-mail: vfish@haystack.mit.edu (VLF); malcolm.gray@manchester.ac.uk (MG); mgoss@aoc.nrao.edu (WMG); a.m.s.richards@manchester.ac.uk (AMSR)

transition with the Multi-Element Radio-Linked Interferometer Network (MERLIN). These observations occurred during a flare event in the 1720-MHz transition. In addition, we investigate the degree to which apparent motions of OH masers are indicative of actual maser motions.

2 OBSERVATIONS

2.1 VLBA

W75N was observed with the VLBA on 2008 February 22 and 2008 April 26. Total time on-source was approximately 1.4 h in February and 6.8 h in April. The original purpose of the observations (experiment code TC013) was to test and validate the output of the DiFX software correlator against the Socorro hardware correlator, but the observations were of suitable quality for scientific purposes as well.

The February observations focused on the 1665- and 1720-MHz transition, while all four ground-state transitions of OH – including 1612 and 1667 MHz – were observed in April. All data were taken in dual circular polarization mode using 125-kHz bandwidths. Data presented in this manuscript were correlated with the Socorro correlator using 128 spectral channels. These parameters correspond to a local standard of rest (LSR) velocity span of 22 km s^{-1} with a channel spacing of 0.18 km s^{-1} at 1665 MHz. Bandwidths were centred on LSR velocities of 6.0 km s^{-1} at 1612 and 1665 MHz and 10.0 km s^{-1} at 1667 and 1720 MHz. The 1612-MHz data produced no detections and were therefore not further analysed.

Data were reduced using AIPS. The source 3C 345 was used as a bandpass calibrator. In each epoch, the data were calibrated using a single spectral channel of a bright maser feature in 1665 MHz left circular polarization (LCP) and another in 1720 MHz right circular polarization (RCP). The resulting solutions were copied over to the other polarization. Data at 1667 MHz were phase-referenced to 1665 MHz. Calibrated data were imaged using natural weighting and 1.5-mas pixel spacing. The synthesized beamwidth was approximately 9 × 6 mas at a position angle near −18° east of north, and the blank sky, single-polarization thermal noise was $\sigma \approx$ 8 mJy beam^{-1} in the April epoch.

2.2 MERLIN

W75N was observed with MERLIN on 2008 May 13–14 in the 1720-MHz transition only (rest frequency 1720.533 MHz). Total on-source time from 16 scans was 15 h and 50 min. Dual circular polarization observations covered a total bandwidth of 500 kHz in 256 spectral channels with 0.34 km s^{-1} spacing. Channel 128 was set to an LSR velocity of 8 km s^{-1}.

The phase calibrator, 2005+403, was observed nearly simultaneously with the target but in a wide-band mode comprising a single 13-MHz channel for greater sensitivity. The flux calibrator 3C 286 and bandpass calibrator 3C 84 were observed in both the narrow spectral line mode of the target and the wide mode of the phase calibrator.

Data were reduced in AIPS. After initial flagging of the calibrator data, the task CALIB was run on both the narrow- and wide-mode data for 3C 84 in order to determine the phase offset between these observing modes, which remained constant over the duration of the observations. The wide-mode phase-calibration table was copied to the narrow-mode data and applied to correct for the phase offset. The narrow-band data for 3C 84 were then calibrated in phase and amplitude, using 17.47 Jy as the flux density in the observing band. The phase calibration consisted of a two-cycle self-calibration of 2005+403 in wide mode.

The RCP data for W75N at 1720 MHz were self-calibrated using the brightest channel. The resulting solutions were then applied to LCP to maintain the flux scale and the relative positional registration between the polarizations. The LCP data were subsequently self-calibrated after zeroing the RCP solutions. During processing, data were weighted according to the sensitivity of each antenna. Natural weighting was then used for imaging, and 1024 × 1024 pixel image cubes were generated. 10 noisy channels were dropped from each end of the frequency range. The synthesized beamwidth was 206 × 142 mas at a position angle of −24°, and the blank sky, single-polarization thermal noise was 3 mJy beam^{-1}.

2.3 Nançay

Brief observations of the 1665- and 1720-MHz lines of OH were conducted with the Nançay Radio Telescope on 2011 January 11. Two scans totalling 7.5 min were observed in dual linear and dual circular polarization. The observing bandwidth of 390.625 kHz was subdivided into 1024 spectral channels, giving a resolution of 0.069 km s^{-1} at 1665 MHz and 0.066 km s^{-1} at 1720 MHz. The observing band was centred near +26 km s^{-1} LSR. Observations were frequency-switched with an offset of half the observing band, making the usable velocity range approximately −8 to +26 km s^{-1}. Data were reduced using CLASS.

2.4 Identification of maser features

In each spectral channel of the AIPS and MERLIN data, maser components detected above 7σ were fitted with the AIPS task ORFIT (based on the standard AIPS task JMFIT) to determine their position, flux density and size. Maser components appearing in consecutive velocity channels and whose centroid positions agree to within a fraction of the synthesized beamwidth are identified as maser features. The two circular polarizations are analysed independently. For each maser feature, Tables 1, 2 and 3 report the centroid position, flux density and LSR velocity of the channel of peak flux density.

The theoretical random error in determining the centroid position of a maser component is approximately the synthesized beamwidth divided by twice the signal-to-noise ratio (Reid et al. 1988), although for an unfilled aperture this is an underestimate by a factor of a few (Richards, Yates & Cohen 1999; see also Condon et al. 1998). Measurement error in determining magnetic field strengths from Zeeman splitting is proportional to the error in determining the velocity of peak emission of the LCP and RCP components of each Zeeman pair, which in turn is dominated by the velocity spacing of spectral channels (0.176 km s^{-1} at 1665 and 1667 MHz and 0.170 km s^{-1} at 1720 MHz for the VLBA observations). This imposes a quantization of the measured magnetic field strengths in units of approximately 0.3, 0.5 and 1.5 mG at 1665, 1667 and 1720 MHz, respectively.

2.5 Alignment of reference frames and flux conventions

The VLBA observations of the 1667-MHz transition are phase-referenced to the 1665-MHz transition. The absolute position of the reference feature at 1665 MHz is determined by identifying it with maser feature A in Slysh et al. (2010), whose location was determined to be $20^{\rm h}38^{\rm m}36\overset{\rm s}{.}4082$, $+42^\circ37'34\overset{''}{.}238$ (J2000) with an error of 2 mas in 2005 September. At 1720 MHz, the MERLIN

Table 1. Detected masers at 1665 MHz.

2008 April					2008 February			2004	2000
RA off. (mas)	Dec. off. (mas)	S_ν (Jy)	$v_{\rm LSR}$ (km s^{-1})	Pol	RA off. (mas)	Dec. off. (mas)	S_ν (Jy)	Feature number	Feature number
−494.89	−428.70	0.08	7.41	R	–	–	–	–	–
−493.42	148.18	0.23	6.88	L	–	–	–	1	1
−492.16	−444.00	0.06	7.41	R	–	–	–	2	–
−491.52	−443.40	0.09	7.41	L	–	–	–	2	2
−300.55	257.63	1.22	6.00	L	−300.56	257.58	1.11	3	3
−289.50	322.25	0.31	6.00	L	–	–	–	–	–
−262.22	−312.48	0.84	12.68	R	−262.51	−313.01	0.76	4	4
−248.49	−1145.77	0.18	9.69	R	–	–	–	5	5
−248.11	−1145.40	0.14	9.69	L	–	–	–	5	5
−110.40	711.29	0.14	8.29	R	–	–	–	8	–
−109.82	711.62	0.20	6.00	L	–	–	–	–	–
−103.41	714.99	0.22	8.29	R	–	–	–	–	–
0.00	0.00	45.10	12.33	R	0.00	0.00	44.95	10	7
0.02	−0.22	1.95	9.16	R	−0.01	−0.25	3.15	9	8
0.10	−0.02	36.38	9.16	L	−0.01	−0.33	50.26	9	8
–	–	–	–	L	0.10	−0.11	0.69	–	–
40.47	66.35	0.44	7.05	L	39.12	64.63	0.60	–	–
42.05	68.20	0.14	7.23	R	–	–	–	–	–
94.00	−86.65	0.15	9.69	R	–	–	–	(13)	–
91.17	−71.43	0.26	13.73	L	–	–	–	12	10
92.29	−59.07	0.06	13.73	L	–	–	–	–	–
106.58	−73.65	0.12	9.69	R	–	–	–	–	–
114.94	−69.53	0.29	9.34	R	–	–	–	14	11
126.45	−56.80	0.06	14.61	R	–	–	–	17	–
129.48	947.26	0.36	3.36	L	129.80	947.71	0.44	–	–
131.03	−67.10	0.25	12.68	L	–	–	–	–	15
138.51	−14.11	0.24	12.86	L	–	–	–	19	16
201.13	718.81	0.40	11.10	R	–	–	–	25	21
201.27	708.55	0.80	10.92	R	–	–	–	26	22
201.51	736.57	0.11	11.10	R	–	–	–	–	–
204.16	726.41	0.08	7.23	L	–	–	–	–	–
204.82	671.94	0.08	8.99	R	–	–	–	29	23
205.25	674.25	0.08	4.42	L	–	–	–	28	24
205.95	1103.09	5.84	5.47	R	206.26	1103.30	2.52	31	26
206.06	1103.49	0.74	5.47	L	206.80	1103.75	0.62	31	–
212.00	1107.10	1.04	5.82	R	–	–	–	32	27
213.15	616.32	0.22	4.59	L	–	–	–	33	–
229.76	582.15	5.67	5.30	L	229.69	582.21	6.81	35	29
230.30	581.80	1.17	5.47	R	230.24	582.47	0.57	35	29
232.55	551.53	0.65	10.04	R	–	–	–	37	–
233.08	1008.85	0.36	5.30	R	–	–	–	39	–
233.57	560.54	16.42	5.47	L	233.48	559.86	12.79	38	–
233.59	560.47	2.38	5.47	R	233.43	559.65	2.23	38	–
233.69	596.00	1.98	10.39	R	234.04	595.80	3.17	–	–
233.78	559.07	0.78	10.04	R	–	–	–	–	–
234.13	584.26	0.38	10.22	R	–	–	–	36	28
234.38	588.46	1.45	5.82	L	–	–	–	–	–
276.55	1113.87	0.55	4.42	L	–	–	–	–	–
277.38	1114.97	0.70	6.53	R	–	–	–	40	30
277.49	1094.61	11.83	5.82	R	277.84	1094.92	8.20	41	32
278.63	1113.82	0.36	4.24	R	278.81	1113.88	0.24	42	31
279.07	1096.29	2.93	5.65	L	279.43	1096.96	2.19	41	32
282.93	1114.59	8.57	4.07	L	282.90	1114.58	5.20	42	33
289.34	1115.25	0.28	5.82	R	–	–	–	–	–
296.55	1111.64	1.51	6.88	R	296.41	1111.93	0.96	43	34
296.68	1144.82	0.18	5.65	L	–	–	–	–	–
297.11	1111.36	0.11	4.42	L	–	–	–	–	–
300.52	1178.84	0.44	3.19	L	300.08	1178.47	0.48	44	36
301.82	1148.25	0.05	7.23	R	–	–	–	45	35
302.06	1178.36	0.47	5.65	R	–	–	–	46	37
302.10	1178.44	0.73	5.65	L	302.39	1178.58	0.87	46	37

Table 1 – *continued*

2008 April RA off. (mas)	2008 April Dec. off. (mas)	S_ν (Jy)	$v_{\rm LSR}$ (km s^{-1})	Pol	2008 February RA off. (mas)	2008 February Dec. off. (mas)	S_ν (Jy)	2004 Feature number	2000 Feature number
322.37	129.46	0.16	8.64	R	–	–	–	–	–
326.40	131.51	0.64	13.91	L	326.61	131.73	0.76	47	38
342.21	1178.75	19.47	5.47	R	342.15	1178.77	14.21	48	40
342.67	1178.55	2.38	5.65	L	342.29	1178.34	2.45	48	40
342.82	780.47	0.08	6.88	R	–	–	–	–	–
343.76	1134.23	0.31	6.53	L	344.21	1134.24	0.30	49	39
343.78	1134.11	1.40	6.53	R	343.91	1134.28	1.27	49	39
346.84	1180.12	0.68	3.36	L	346.49	1180.49	0.54	50	–
366.68	1148.67	0.33	4.59	L	366.55	1148.14	0.37	51	–
368.15	1151.27	0.11	7.05	R	–	–	–	52	–
401.26	1229.21	0.06	7.05	R	–	–	–	–	–
401.75	1231.33	0.42	4.77	L	401.65	1230.54	0.45	53	41
421.41	1251.55	0.17	5.12	L	–	–	–	–	–
439.11	1258.69	0.29	5.47	L	–	–	–	–	–
443.98	1278.14	1.61	5.12	L	444.22	1278.27	1.30	54	42
444.96	1278.65	0.31	5.12	R	–	–	–	54	42
456.51	1292.55	5.93	5.12	L	457.75	1293.74	6.18	55	43
457.01	1293.31	3.42	5.12	R	457.25	1293.31	2.88	55	43
460.53	1296.87	3.61	5.30	L	–	–	–	–	–
482.67	1344.21	0.14	4.95	R	–	–	–	56	–
482.83	1344.49	2.07	4.95	L	482.96	1343.97	1.68	–	45
490.16	1349.03	6.01	5.12	L	490.80	1349.39	6.18	–	–
490.46	1349.80	0.46	7.23	R	490.42	1350.17	0.46	57	44
490.93	1349.27	0.71	5.30	R	490.81	1349.62	0.81	58	45
532.53	1450.88	0.10	7.05	R	–	–	–	59	46
548.39	1494.14	0.35	6.18	R	–	–	–	60	48
551.21	1498.99	6.43	3.71	L	550.84	1499.18	5.39	61	49
555.60	1512.50	0.10	6.18	R	–	–	–	–	50
602.73	−97.60	0.10	3.19	R	–	–	–	62	52
604.17	−98.34	0.07	3.19	L	–	–	–	62	52
–	–	–	–	L	703.30	−198.98	2.24	–	–
722.24	−175.64	0.25	16.20	L	–	–	–	–	–
726.76	−132.36	0.29	−0.86	L	–	–	–	–	–
730.11	−199.21	0.98	11.27	R	730.19	−198.96	3.12	–	–
730.45	−198.92	0.68	11.27	L	–	–	–	–	–
–	–	–	–	R	737.67	−130.51	1.56	–	–
737.75	−128.49	2.91	−0.50	L	739.15	−127.99	1.35	–	–
738.05	−128.53	1.60	−0.50	R	739.13	−128.07	0.73	72	–
–	–	–	–	R	738.06	−139.43	2.39	–	–
–	–	–	–	L	738.45	−141.27	3.31	–	–
740.38	−152.14	0.16	16.37	L	–	–	–	–	–
741.08	−147.91	43.21	1.96	L	741.17	−148.09	44.99	70	–
741.42	−147.68	24.28	1.78	R	741.41	−147.77	23.53	70	–
741.95	−152.95	67.91	−0.15	R	741.71	−152.78	58.47	71	–
742.00	−152.89	279.86	−0.15	L	741.72	−152.74	213.96	71	–
–	–	–	–	L	744.98	−157.38	6.77	–	–
–	–	–	–	R	745.24	−157.51	1.66	–	–
745.28	−135.81	2.10	0.02	R	745.50	−135.51	2.14	73	–
754.08	−81.73	1.94	7.93	L	754.02	−81.97	5.75	–	–
754.36	−82.29	0.13	7.93	R	753.88	−81.95	0.60	–	–
791.08	−240.26	0.89	5.82	L	791.92	−240.58	0.60	–	–
792.01	−240.73	20.79	5.82	R	791.90	−241.28	16.50	82	–
801.73	−134.88	0.32	3.36	L	–	–	–	–	–
802.12	−134.72	0.29	3.36	R	–	–	–	–	–
813.86	−137.85	0.11	3.54	L	–	–	–	–	–
814.00	−117.46	1.15	1.78	R	–	–	–	–	–
817.15	−121.02	0.07	3.54	L	–	–	–	–	–
818.16	−121.13	0.09	3.71	R	–	–	–	–	–
844.63	−1290.71	0.10	10.39	R	–	–	–	–	–
1343.27	50.88	0.27	11.45	L	–	–	–	85	–
1343.29	50.62	0.24	11.45	R	1342.93	51.59	0.28	85	–

Table 1 – *continued*

2008 April RA off. (mas)	2008 April Dec. off. (mas)	2008 April S_v (Jy)	2008 April v_{LSR} (km s^{-1})	Pol	2008 February RA off. (mas)	2008 February Dec. off. (mas)	2008 February S_v (Jy)	2004 Feature number	2000 Feature number
1705.89	−590.11	0.56	13.73	R	1706.08	−590.47	0.53	86	76
1784.55	−585.60	0.14	16.20	L	–	–	–	88	–
1784.67	−596.26	7.99	11.98	R	1785.50	−596.35	4.81	89	78
1784.89	−596.30	0.54	12.15	L	1785.14	−596.65	0.33	89	78
1798.07	−598.13	2.20	11.98	R	1796.05	−598.82	0.73	–	79
1812.47	−609.78	0.22	11.98	R	–	–	–	–	–

Table 2. Detected masers at 1667 MHz.

2008 April RA off. (mas)	2008 April Dec. off. (mas)	S_v (Jy)	v_{LSR} (km s^{-1})	Pol	2004 Feature number	2000 Feature number
0.46	−1.29	0.10	10.00	L	91	81
0.68	−2.57	0.07	11.93	R	90	80
102.06	207.73	0.28	10.00	L	92	84[a]
127.87	−56.33	0.32	12.63	L	93	85
127.91	−56.82	0.09	14.21	R	–	–
128.40	−55.55	0.14	12.63	R	93	85
202.46	708.84	1.11	10.00	R	98	92
207.05	674.33	2.29	5.43	L	101	93
207.27	674.04	0.35	8.07	R	102	94
220.16	617.02	0.38	5.26	L	104	–
220.59	616.61	0.09	8.07	R	103	–
221.97	655.89	3.30	5.96	L	105	97
232.91	560.79	0.13	6.49	R	–	–
233.17	560.93	0.43	6.31	L	–	–
233.56	551.78	0.42	6.49	L	107	–
233.84	553.89	0.11	9.12	R	106	–
234.24	594.13	0.39	9.47	R	–	–
235.04	586.21	0.07	6.66	R	–	–
458.15	1294.89	0.16	6.14	R	108	98
463.91	1299.16	0.07	5.79	L	109	–
491.80	1352.32	0.49	5.61	L	111	99
741.41	−149.01	0.59	6.31	L	–	–
746.64	−142.63	10.99	1.40	L	115	–
746.76	−142.93	25.11	1.22	R	115	–
746.82	−160.84	44.10	5.08	L	–	–
746.90	−161.32	13.06	4.91	R	–	–
755.39	−159.48	0.16	2.63	L	–	–
756.52	−148.27	0.16	−0.01	L	–	–
777.82	−110.83	0.75	6.49	L	–	–
779.13	−111.74	8.34	0.52	R	–	–
795.04	−28.92	0.07	10.70	L	–	–
804.93	−111.44	0.19	2.98	R	–	–
811.13	−115.66	0.22	3.33	R	–	–
812.19	−112.55	0.17	4.38	R	–	–
1781.81	−583.39	0.34	15.44	L	120	116
1783.87	−584.66	0.27	12.98	R	121	117
1826.12	−588.85	0.16	12.63	R	–	118
1833.13	−561.60	0.26	14.74	L	122	119
1833.43	−561.64	1.07	12.46	R	123	120

[a]Blended with 83.

Table 3. Detected masers at 1720 MHz with the VLBA.

2008 April RA off.[a] (mas)	2008 April Dec. off. (mas)	S_v (Jy)	v_{LSR} (km s^{-1})	Pol	2008 February RA off. (mas)	2008 February Dec. off. (mas)	S_v (Jy)
110.05	234.34	2.87	9.83	L	110.03	233.92	1.52
110.22	234.46	0.64	11.02	R	110.24	234.49	0.61
125.45	202.79	0.79	11.19	R	–	–	–
125.60	202.94	0.68	10.17	L	125.66	203.27	0.39
–	–	–	7.96	R	177.28	462.60	0.32
177.65	463.27	5.59	6.94	L	177.98	463.92	8.25
178.82	471.93	3.28	9.15	R	–	–	–
–	–	–	8.98	L	182.58	480.81	2.07
184.11	353.33	0.31	8.81	L	–	–	–
184.12	353.95	1.66	9.66	R	184.57	354.94	1.64
185.22	495.08	88.55	8.47	R	–	–	–[b]
185.42	488.00	301.46	8.47[c]	R	185.419	488.000	439.71
185.68	488.04	81.73	7.28	L	185.28	487.62	66.81
185.60	499.28	9.74	7.79	L	185.84	499.40	7.76
–	–	–	9.66	L	186.29	489.70	14.14
189.55	376.55	2.75	11.02	L	189.89	376.70	1.80
192.82	387.85	0.44	10.51	L	193.96	390.29	0.51
197.60	441.05	0.42	9.15	L	–	–	–
210.36	391.62	24.26	8.98	L	210.38	391.72	8.64
–	–	–	8.13	R	210.38	143.35	0.91
210.39	391.99	2.22	10.00	R	210.43	391.62	4.28
211.39	405.84	2.18	9.83	R	–	–	–
214.02	400.60	64.37	9.66	L	214.20	400.58	66.46
217.03	433.22	0.72	9.83	R	–	–	–
217.24	433.86	1.16	8.81	L	216.53	433.30	0.74
219.51	152.90	0.35	7.79	R	219.90	152.46	0.34
221.52	403.23	6.34	9.66	L	–	–	–
223.61	404.14	2.78	9.66	R	224.14	404.83	2.16

[a]The 1720-MHz masers have been put into the 1665/1667-MHz reference frame using the absolute position of the 1720-MHz reference feature and the coordinates of spot A in Slysh et al. (2010) as described in Section 2.5.
[b]Blended with the next spot.
[c]Based on the MERLIN observations, the position of this maser is $20^h38^m36^s.425 + 42^\circ37'34''.73$ (J2000) with a positional uncertainty of 20 mas.

observations obtained a position of the bright reference feature. This position is used to align the VLBA 1720-MHz data relative to the 1665- and 1720-MHz positions.

Throughout this paper, we report flux densities using the AIPS convention [$I = (RR + LL)/2$]. The Nançay data are treated similarly for consistency, although we note that this convention differs by a factor of 2 from that which is sometimes used to report the Nançay data.

3 RESULTS

3.1 VLBA

Counting LCP and RCP features separately, we identify 61 maser features at 1665 MHz in the February data and 121 in the April data. At 1720 MHz, we identify 20 features in the February data and 24 in the April data, although spatial and spectral blending of

the numerous features in a small (approximately 125 × 350 mas) region makes it difficult to uniquely and unambiguously identify some features. In the 1667-MHz transition, observed only in April, we identify 39 maser features.

Parameters of the detected masers are given in Tables 1, 2 and 3 for 1665-, 1667- and 1720-MHz masers, respectively. Images of the April main-line and 1720-MHz data are shown in Figs 1 and 2. Spectra of the recovered emission (i.e. the total flux density in all maser components as determined by fitting elliptical Gaussians) are shown in Fig. 3.

The overall distribution of the 1665- and 1667-MHz maser features in the 2008 epochs is very similar to those of the 2000/2001 and 2004 epochs (Fish et al. 2005; Fish & Reid 2007a). Masers are located in an arc to the north, an elongated cluster near the edge of VLA 1, several small clusters near the origin in Fig. 1, a large cluster on the north-west edge of VLA 2 and a smaller set of masers to the east. In addition, isolated maser spots appear throughout the source, with many having counterpart identifications in previous epochs.

Magnetic field strengths are also broadly consistent from epoch to epoch, with the exception of the cluster near VLA 2. Slysh et al. (2010) note that the masers in this region exhibit significant variability on time-scales of a few months. Masers that are detected in one epoch may no longer be detectable a few months later, in

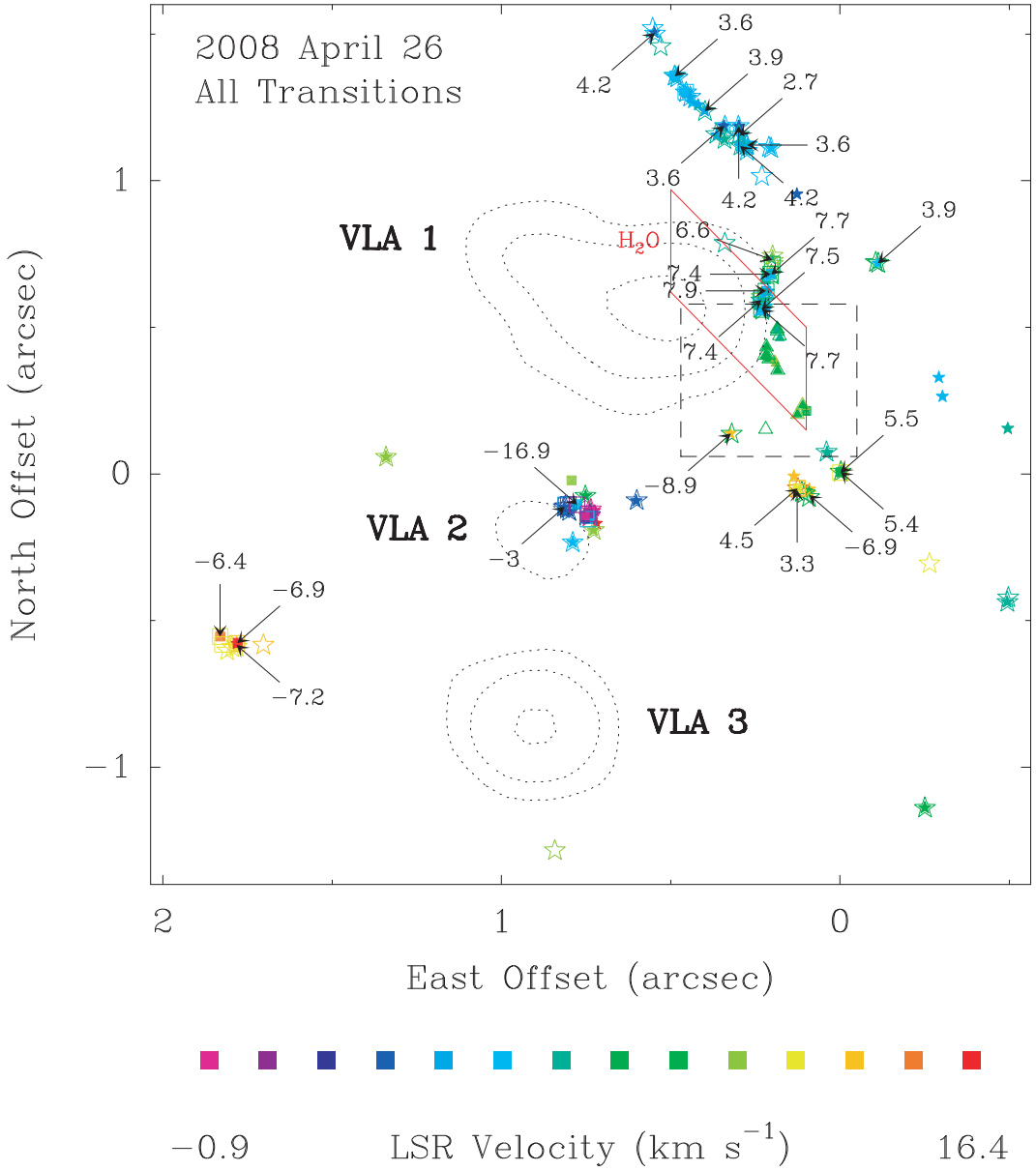

Figure 1. Image of detected OH masers in the 2008 April 26 data. Stars, squares and triangles indicate 1665-, 1667- and 1720-MHz masers, respectively. LCP features are shown as filled symbols, and RCP features are shown as larger, open symbols, with colour used to indicate LSR velocity. Not all known maser features in W75N fall within the velocity range of our observations (see Fish et al. 2005). Numbers indicate magnetic field strengths in milligauss as determined from 1665- and 1667-MHz Zeeman pairs (see Fig. 2 for 1720-MHz Zeeman pairs). Continuum emission at 8.4 GHz is shown in dotted contours (Argon, Reid & Menten 2000; Fish & Reid 2007a). The position of the reference feature at the origin was measured in 2005 September to be $20^{h}38^{m}36\overset{s}{.}4082$, $+42^{\circ}37'34\overset{''}{.}238$ (J2000) (Slysh et al. 2010). All detected 1720-MHz masers appear in the region inside the dashed box, which is shown in greater detail in Fig. 2. The red parallelogram shows the region in which the highly variable water masers associated with VLA 1 appear (Torrelles et al. 1997; Lekht, Slysh & Krasnov 2009).

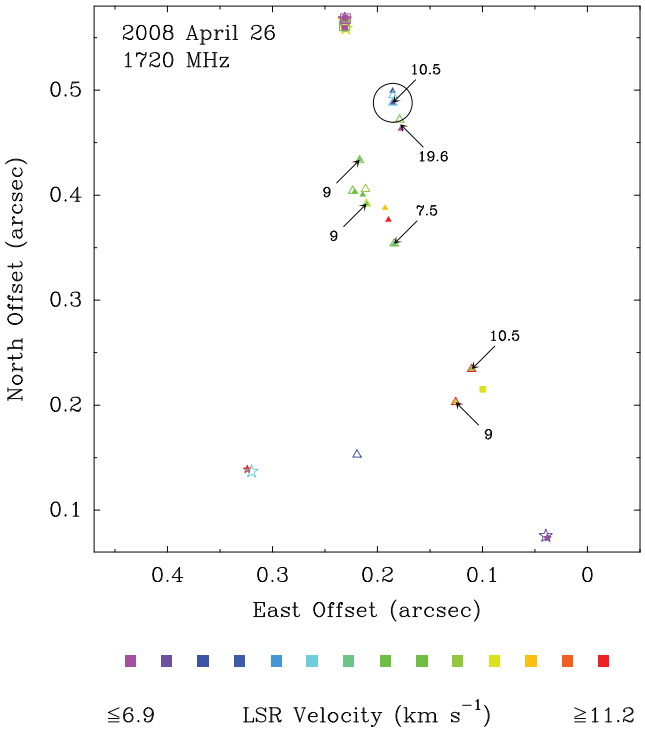

Figure 2. Enlargement of detected 1720-MHz OH masers in the 2008 April 26 VLBA data. The black circle denotes the location of the brightest maser. The velocity scale is different from that of Fig. 1. The origin is located at $20^{\rm h}38^{\rm m}36\overset{\rm s}{.}4082$, $+42^\circ37'34\overset{''}{.}238$ (J2000), and the relative registration uncertainty between the 1665/1667-MHz and the 1720-MHz features is ∼20 mas.

which time new masers may have appeared. The VLA-2 region also contains numerous masers without an obvious Zeeman counterpart in the opposite polarization. Consequently, there are comparatively fewer Zeeman magnetic field measurements in this region than in the other clusters in W75N. As in previous epochs (Slysh & Migenes 2006; Fish & Reid 2007a; Slysh et al. 2010), the largest main-line magnetic field strength detected in these observations, approximately 17 mG, occurs in VLA 2. (However, our narrow observing bandwidth does not rule out the possibility of Zeeman pairs implying larger magnetic field strengths.)

In addition, for the first time, we present a VLBI image of the 1720-MHz masers in W75N (Fig. 2). Unlike the main-line masers, which are found throughout W75N, the 1720-MHz masers are found only between the group of masers on the western edge of the continuum emission from VLA 1 and the cluster of masers near the origin of Fig. 1 (to the south-west of VLA 1). The magnetic fields deduced from Zeeman splitting at 1720 MHz are all several milligauss higher than those derived from the 1665- and 1667-MHz transitions. The line-of-sight direction of the magnetic field at the 1720-MHz sites is oriented away from the observer everywhere that it is detected, which is consistent with the direction implied by the vast majority of the 1665- and 1667-MHz masers detected north of the reference feature (at the origin in Fig. 1).

Most of the 1720-MHz masers detected in one of the two 2008 epochs were detected in the other and found to have similar intensity (to within a few tens of per cent). The differences between the two epochs can largely be explained by the difficulty of identifying as separate, maser components that are spatially blended (i.e. within a synthesized beamwidth for most spots or more for the brightest

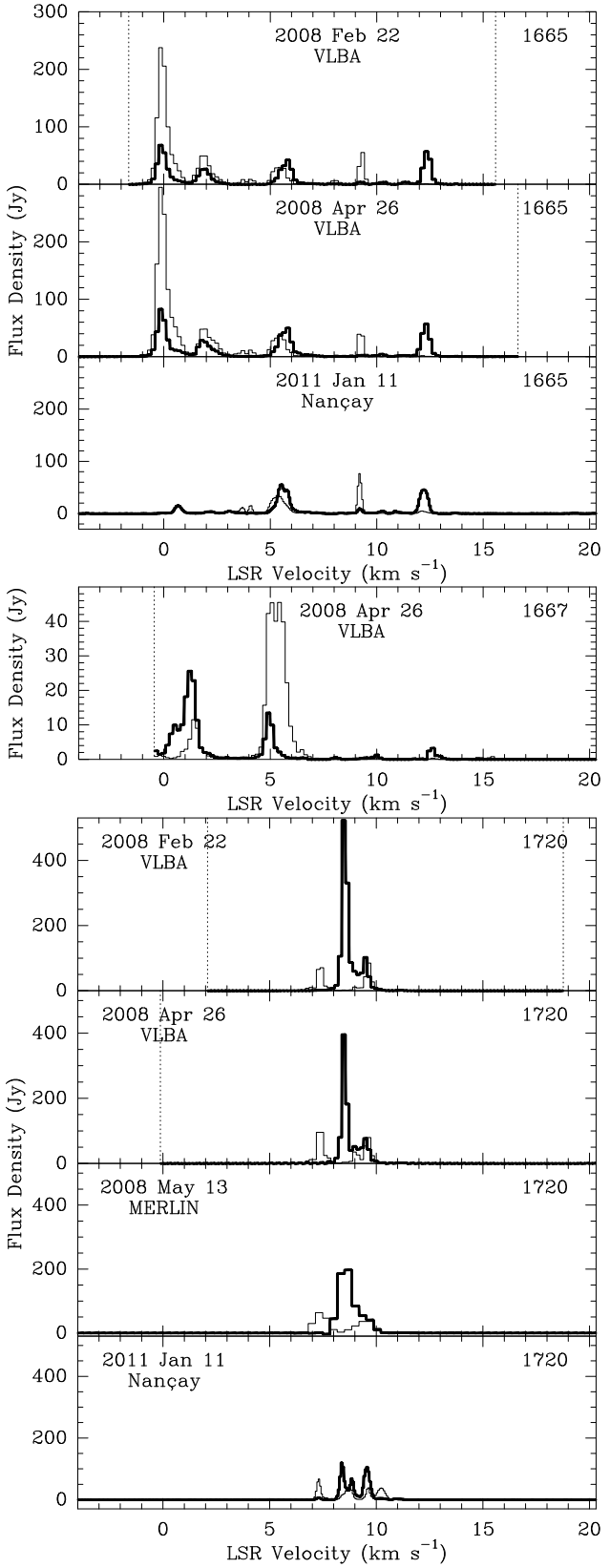

Figure 3. Spectra of the maser emission at 1665 (top), 1667 (middle) and 1720 MHz (bottom). RCP and LCP emission are shown in bold and normal weight, respectively. Dotted lines denote the last velocity channel imaged. Spectra of the integrated maser emission from the May MERLIN data have coarser velocity resolution.

spots, where the noise is higher than thermal noise due to imperfect calibration and deconvolution of the bright maser spot) or spectrally blended (i.e. a secondary peak in the spectrum of a bright maser located at roughly the same location but at a different velocity).

3.2 MERLIN

The MERLIN observations were made with the primary aim of determining an accurate absolute position for the flaring maser object at 1720 MHz. The position of the brightest (189 Jy beam^{-1}) RCP maser feature, measured before self-calibration, was $20^{\rm h}38^{\rm m}36\overset{\rm s}{.}425$, $+42^\circ37'34\overset{''}{.}73$ (J2000). The uncertainty in this position is dominated by effects related to the phase calibration and has three main contributions: ∼5 mas from the uncertainties in the geographical positions of the MERLIN telescopes, a contribution from the uncertainty in the position of the phase calibrator itself (0.6 mas; Petrov, unpublished[1]), and a contribution dependent on the angular separation between the phase calibrator and target (8°), owing to the small difference in atmospheric conditions between the two sources. Assuming a positional uncertainty of 2 mas deg^{-1} from the latter effect, the astrometric accuracy is 17 mas.

We can identify the brightest MERLIN feature, introduced above, with the brightest RCP 1720-MHz feature from the April VLBA data (feature 12 in Table 3) with confidence. At a typical maser velocity of 10 km s^{-1}, this feature would have moved a distance of less than 0.1 mas over the 18 days separating the April VLBA and MERLIN observations. The MERLIN position is used to align the 1720-MHz VLBA reference frame with the 1665/1667-MHz frame, identifying the 1665-MHz reference feature as feature A in Slysh et al. (2010), whose position was determined to 2-mas accuracy in 2005 September by phase-referencing European VLBI Network (EVN) observations of the OH masers to a nearby calibrator.

The flux densities of individual maser spots in the MERLIN data are not directly comparable with those in the VLBA data due to the lower spectral and spatial resolution. However, the integrated flux densities of all epochs can be compared. The integrated Stokes *I* flux density of the MERLIN data, 307 Jy km s^{-1}, is approximately the same as measured in each of the VLBA epochs (310 and 271 Jy km s^{-1} in February and April, respectively) to within flux scale uncertainties.

3.3 Variability

The most striking feature of the 1720-MHz data is the bright flare producing a peak flux density exceeding 400 Jy (in an RCP 8.5 km s^{-1} feature). Bright features exceeding 60 Jy are also detected at 7.3 and 9.7 km s^{-1}, with numerous other masers of a few Jy or brighter detected over an LSR velocity range of ∼4 km s^{-1}. Flux densities were approximately persistent over a period of three months in 2008 both on a spot-by-spot (Table 3) and an integrated flux density basis (Section 3.2). The bright flare weakened between the 2008 MERLIN epoch and the Nançay observations in 2011.

In contrast, only three 1720-MHz maser features were detected with the MERLIN array in 1993, with peak intensities of 3.7, 0.3 and 0.2 Jy beam^{-1} (Hutawarakorn et al. 2002). We do not detect any of these features, although the latter two may be below our sensitivity limit. The locations of these masers would be located near the southern 1720-MHz masers in Fig. 2.

[1] Available at http://astrogeo.org/vlbi/solutions/rfc_2010c.

Flares in W75N also occur in the 1665-MHz transition (Alakoz et al. 2005), with total emission from masers near 0 and 2 km s^{-1} exceeding a flux density of 1000 Jy at their brightest (Slysh et al. 2010). These masers are located near the continuum source VLA 2. In 2008, the 0 km s^{-1} feature exceeded 200 Jy LCP and the 2 km s^{-1} feature exceeded 40 Jy LCP. By 2011, the flux densities of these features had dropped to the ∼1 Jy level, although a 15–20 Jy feature appeared near 0.7 km s^{-1}. In contrast, the flux densities of features with $v_{\rm LSR} \gtrsim 3$ Jy are much more stable over the 3 years of observations.

At 1667 MHz, Slysh et al. (2002) detected a 21-Jy feature at 9.8 km s^{-1}, which had weakened substantially by the epochs reported on in Slysh et al. (2010). The RCP feature near 15 km s^{-1} brightened by nearly an order of magnitude between 2006 March and 2007 July but is not detected in our data (although a much weaker LCP feature is detected). We detect bright 1667-MHz masers near 1.2 km s^{-1} (25 Jy RCP and 11 Jy LCP) and 5 km s^{-1} (44 Jy LCP and 13 Jy RCP), which correspond to weaker masers detected in the 2007 July epoch of the Slysh et al. (2010) Kalyazin RCP spectra but not in the 2006 March or July epochs (although the 5 km s^{-1} feature may be very weakly present in the latter), indicating that these features were starting to brighten 1 year before our observations. Both the 1.2 and 5 km s^{-1} features are located near VLA 2.

3.4 Comparison with previous VLBI data

Almost all of the masers reported by Slysh et al. (2010) have identifiable counterparts in our data. At 1665 MHz, they detected 32 maser features in one of their 2006 epochs within the velocity range of our 2008 April observations, excluding masers near VLA 2. We find corresponding masers in our data within a few milliarcseconds – and in almost all cases, within a few tenths of a km s^{-1} – of the position and velocity given in table 1 of Slysh et al. (2010). We also find masers within a few milliarcseconds of the locations of several of the Slysh et al. (2010) masers associated with VLA 2, although the masers in this region are highly variable. At 1667 MHz, Slysh et al. (2010) report on 12 masers in our velocity range, excluding the VLA-2 region. We find masers near 11 of these locations.

In the other direction, a substantial fraction of the masers we report do not have counterparts listed in Slysh et al. (2010). A direct, one-to-one comparison of maser spots is made difficult by the non-identification of polarization information in the Slysh et al. (2010) data. For instance, some of the masers we detect may correspond to Zeeman counterparts of masers listed in the tables in Slysh et al. (2010). Other discrepancies may be due to methodological differences in the data reduction. Where masers are close enough together for their emission to appear spatially blended at the resolution of our array, we have attempted to fit two – or rarely more – elliptical Gaussians to the emission.

3.5 Magnetic fields

The magnetic fields derived from the 1665- and 1667-MHz VLBA observations are consistent in magnitude and line-of-sight direction with values obtained in previous observations in all clusters of maser spots, with the caveat that there is a large range of measured field values near VLA 2 (Fish et al. 2005; Fish & Reid 2007a). At 1720 MHz, we detect several Zeeman pairs of approximately 9 mG as well as one Zeeman pair indicating a field strength of about twice this value.

The magnetic field strengths we report at 1720 MHz are higher than the magnetic field reported by Hutawarakorn et al. (2002) for Zeeman pair Z_6. It is difficult to identify exact counterparts to the Hutawarakorn et al. (2002) detections in our VLBA data due to the much lower angular resolution of the MERLIN data and significant flaring in the intervening 15 years between the observations. Nevertheless, we do find a Zeeman pair at approximately the same velocity as Hutawarakorn et al. (2002) and with the same sense and approximate magnitude of the velocity separation ($v_{\rm RCP} - v_{\rm LCP} = 1.0\,{\rm km\,s^{-1}}$). Hutawarakorn et al. (2002) interpret this as due to a +4.6-mG magnetic field, while we identify the field strength as +9 mG. The difference may arise due to uncertainty in the Zeeman splitting coefficient for satellite-line masers. Davies (1974) provides the splitting coefficient appropriate if the LCP and RCP features are due to a blend of the $\sigma^{\pm1}$, $\sigma^{\pm2}$ and $\sigma^{\pm3}$ components in the intensity ratio expected in local thermodynamic equilibrium. However, very high spatial and spectral resolution observations of the brightest 1612- and 1720-MHz OH masers in W3(OH) uncovered no evidence for contributions of the $\sigma^{\pm2}$ and $\sigma^{\pm3}$ components (Fish, Brisken & Sjouwerman 2006). The Zeeman splitting coefficient appropriate for the $\sigma^{\pm1}$ components is half that appropriate for the blend of all components, resulting in an estimate of the magnetic field that is twice as large.

3.6 Maser motions

Fig. 4 shows the apparent relative maser motions between the 2004 and 2008 epochs. The reference frame has been chosen such that the 1665-MHz reference feature at the origin is stationary. The absolute motion of the reference feature cannot be determined from our observations, since the VLBA data were not phase-referenced to a nearby calibrator.

The main features in the apparent motions between 2004 and 2008 agree with the main features in the motions between 2000/2001 and 2004 (Fish & Reid 2007a). Relative to the reference spot at the origin, the northernmost masers are moving northwards, possibly streaming along the curve that outlines their general distribution. The cluster of masers at the western edge of the VLA-1 continuum region also show net northward motion in both epochs. The isolated masers found to the west and south of the reference feature display net motion westwards. The general patterns of motions near VLA 2 and in the easternmost cluster of masers are less clear. We conclude that the general pattern of motions is consistent with Fish & Reid (2007a) and explore the apparent differences statistically in Section 4.3.

4 DISCUSSION

4.1 Environment of the flaring 1720-MHz masers

Strong flares in the 1665-MHz transition (Alakoz et al. 2005; Slysh et al. 2010) and weaker flares in the 1667-MHz transition (Section 3.3) are observed in the vicinity of the continuum source VLA 2, a region where the OH masers are rapidly variable and trace large magnetic fields (Slysh & Migenes 2006; Fish & Reid 2007a). In contrast, the bright 1720-MHz flare on which we report is located ∼1000 au away from VLA 2.

It is difficult to say definitively whether the 1665/1667- and 1720-MHz flares are correlated, since the 1720-MHz transition has not been monitored in W75N to nearly the same extent as the main-line transitions. If the flares are correlated, the flare excitation process cannot be due to the passing of an MHD shock wave, which would require ∼500 yr to cross from one site to the other at $10\,{\rm km\,s^{-1}}$. Alternatively, the 1665/1667- and 1720-MHz flares could be excited by a radiative mechanism, which can couple the region in less than 6 days. However, the correlation, if it exists, is not very tight, since the 1665-MHz feature at $0\,{\rm km\,s^{-1}}$ increases in intensity, whilst the flaring 1720-MHz feature decreases

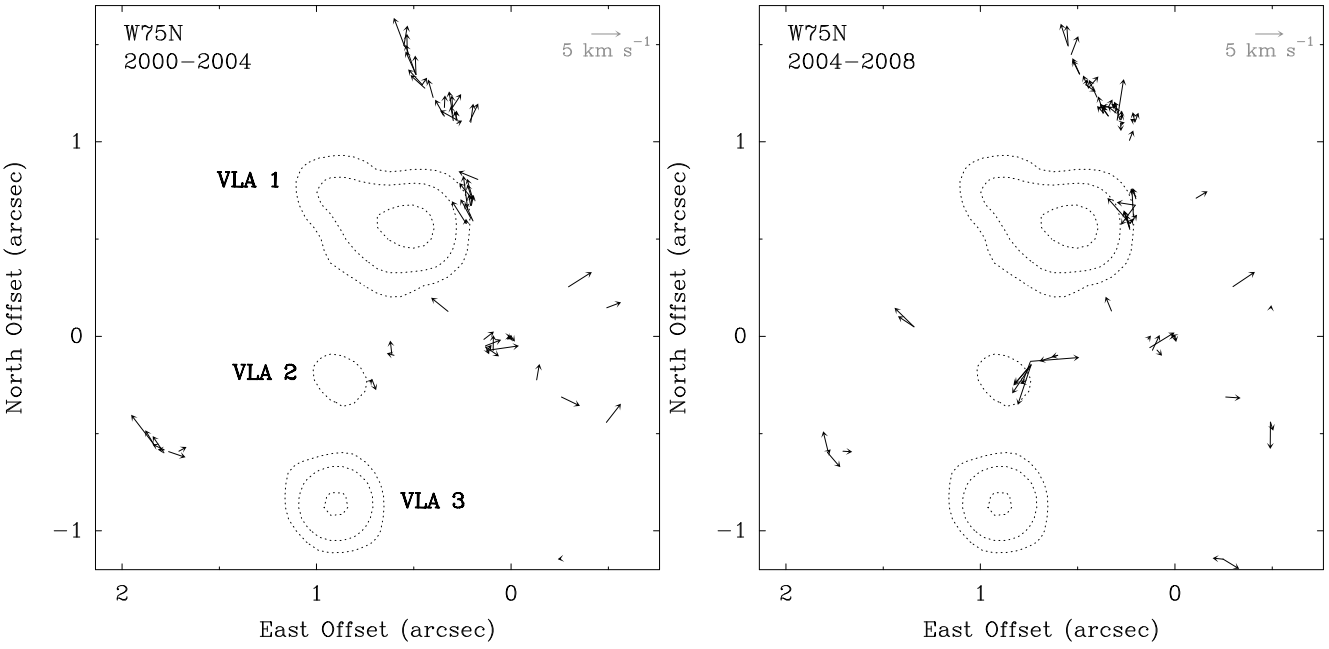

Figure 4. Apparent proper motions of masers in W75N between 2000 and 2004 (left), and between 2004 and 2008 (right). The left-hand panel shows the proper motions from Fish & Reid (2007a) in the reference frame of the 2008 data (i.e. keeping the 2008 reference feature stationary) after rescaling to a distance of 1.3 kpc (Rygl et al. 2010) but removing the misidentified $50\,{\rm km\,s^{-1}}$ motion (see Slysh et al. 2010). A proper motion of $5\,{\rm km\,s^{-1}}$ corresponds to an apparent change in position of $0.8\,{\rm mas\,yr^{-1}}$.

slightly between 2008 February and April (Fig. 3). It is therefore more plausible that the flaring events near VLA 1 and VLA 2 are unconnected.

Instead, the 1720-MHz OH masers are likely associated with the 22-GHz water masers. The 1720-MHz masers are located near the edge of the continuum source VLA 1, aligned with water masers that lie along a line oriented north-east–south-west through the continuum source (Torrelles et al. 1997). Like the 1720-MHz OH masers, the 22-GHz H_2O masers exhibit extreme variability. Water masers appear and disappear on time-scales of a year or less, with one feature reaching a flux density of around 4000 Jy, becoming two orders of magnitude fainter in 2 years and then returning to over 1000 Jy a few years later (Felli et al. 2007; Lekht et al. 2009).

4.2 Models of the 1720-MHz masers

Torrelles et al. (1997) interpret the continuum emission from VLA 1 as being due to a radio jet, noting that the presence of water masers along this axis is consistent with this interpretation. Based on the lack of a clear velocity gradient in the LSR velocities of the water masers along this axis, they speculate that the water masers are shocked by the jet but not accelerated by it to any great degree, suggesting that the water masers are embedded in dense clumps of material. The LSR velocities of the H_2O masers on the south-east side of VLA 1 range from 10 to 16 km s^{-1}, which is close to the velocity of the ambient material as traced by CS (10 km s^{-1}; Hunter et al. 1994). The relatively small velocity difference likely implies that the water masers reside near the interface of the radio jet with the ambient material and are pumped by the turbulent cascade of energy from the large-scale outflow to the scale of individual water masers (Strelnitski et al. 2002).

The properties of the OH masers fit this model. The velocity range of the 1720-MHz masers is 7 to 11 km s^{-1}, overlapping both the velocity range of the water masers and the velocity of the ambient material. The magnetic fields measured by 1720-MHz Zeeman splitting, up to 20 mG, are about three times larger than usual for OH masers in star-forming regions, suggesting that the material that they trace is a factor of $\sim$10 denser under the usual assumption that density is correlated with magnetic field strength ($B \propto n^{\alpha}$, $\alpha \approx 0.5$; Crutcher 1999). The existence of flaring OH masers in the 4765-MHz transition in this region (Niezurawska et al. 2004) also supports a high density. Gray, Field & Doel (1992) find that strong 1665-MHz maser emission can arise at $n_{\rm OH} \approx 20\,{\rm cm}^{-3}$, while at $n_{\rm OH} \geq 200\,{\rm cm}^{-3}$ strong 1720- and 4765-MHz emission is seen without accompanying 1665-MHz emission (see their fig. 12). The existence of a substantial region of parameter space where the 1720- and 4765-MHz masers coexist at OH specific column densities that are too high for the 1665- and 1667-MHz masers is also supported by Cragg, Sobolev & Godfrey (2002). On the assumption that the number density of OH is a good proxy for the total number density, these models are also consistent with the ratio of densities in the two masing regions as derived from the magnetic field strengths.

The distribution of 1720-MHz OH masers along the line of water masers argues in favour of the 1720-MHz OH masers being associated with an outflow rather than a disc. In this regard, the outflow model of W3(OH) (Gray et al. 1992) may be more directly applicable to the 1720-MHz masers in W75N than the disc model of Gray, Hutawarakorn & Cohen (2003). The W3(OH) model produces 1720- and 4765-MHz OH maser emission near the base of an outflow and 1665-MHz emission farther out, which is observationally consistent with the location of OH masers in W75N along the outflow near VLA 1 as well. However, an important difference between W3(OH) and W75N is that in the former the 1720-MHz masers are intermixed with masers at 1665 MHz, while in the latter the 1720-MHz region is devoid of 1665-MHz masers. More quantitatively, there exist 1665–1720 MHz pairs separated by only a few astronomical units in W3(OH) (Fish et al. 2006), while the separation of the closest such pair in W75N exceeds 100 au. For comparison, there exists a weak 1667-MHz maser located $\sim$30 au from the nearest 1720-MHz maser in W75N.

The non-overlap of 1665- and 1720-MHz masers in W75N may be explained by a larger density than in W3(OH). In a slowly accelerating flow (velocity gradient of 1000 km s^{-1} pc^{-1}, or $\sim$0.3 km s^{-1} per 10^{13} m), competitive gain produces strong 1720-MHz emission while quenching 1665-MHz emission (Gray et al. 1992). W75N is believed to be younger than W3(OH), and the density of molecular material near the H II region is likely to be higher, making competitive gain effects more important in W75N than in W3(OH) (see discussion in Gray et al. 2003). Along the direction of the flow, the first ground-state maser to appear beyond the end of the 1720-MHz maser zone is a weak 1667-MHz maser, followed much farther out by a weak 1665-MHz maser and then by strong 1665-MHz maser emission (the reference feature). The magnetic field strengths falls off from about 9 mG at the end of the 1720-MHz region to 5.5 mG at the location of the bright 1665-MHz emission farther along the flow, indicating that the density decreases by about a factor of 3 away from the H II region. These observed properties are consistent with the various Gray et al. models, which predict that as the gain length increases, the 1720-MHz masers will be produced, while first the 1665-MHz masers and then the 1667-MHz masers are quenched.

4.3 Measurement of proper motions

The recent six-epoch data set of Slysh et al. (2010) highlighted the importance in estimating the magnitude of random errors in determining the positions – and hence apparent proper motions – of OH masers in star-forming regions. Previous proper motion measurements of the 1.6-GHz masers based on two epochs of data (e.g. Fish & Reid 2007a for W75N and Bloemhof et al. 1992 and Fish & Reid 2007b for other sources) do not have the ability to discriminate between true maser motions and non-real apparent motions caused by both random (e.g. thermal noise) and systematic (e.g. deconvolution) errors (Section 2.4). An additional complication is that maser proper motions are typically assumed to be linear, yet real masers may undergo accelerations that produce non-linear trajectories. Turbulence may further complicate interpretation of apparent proper motions.

Slysh et al. (2010) demonstrate that the total of these effects can be much larger than what would be expected from the random uncertainty due to thermal noise alone. The error in determining the maser position can be dominated by other effects, such as calibration and deconvolution errors or changes in the maser substructure on spatial scales smaller than the VLBA resolution of $\sim$7 mas at 1.6 GHz (Fish & Sjouwerman 2007). A discussion of the difficulty in identifying the 'peak' of a maser in a different context can be found in Moellenbrock, Claussen & Goss (2009). On the other hand, the reproducibility of the general features of the 1665-MHz OH proper motions both in W3(OH) (Wright et al. 2004) and W75N (Fig. 4) suggests that apparent maser proper motions, when viewed as an ensemble, are reliable estimators of motions of maser clusters provided that a sufficiently long time baseline has elapsed.

One estimate of these errors can be obtained by comparing the positions of masers in the 2008 February and April data. At 1665 MHz, 54 features are detected in both the February and April

data. Of these, all but six have centroids that agree to better than 1 mas (equivalently, a false apparent proper motion of 36 km s^{-1}) between the two epochs, with a median position difference of 0.4 mas (15 km s^{-1}) after referencing to the same bright maser spot. The position differences between the 2008 February and April epochs provide an estimate of the total error in determining maser proper motions. These are not indicative of true proper motions, since the implied velocities far exceed those measured between 2000 and 2004 (Fish & Reid 2007a), and between 2004 and 2008 April (in this work, median velocity is 3.5 km s^{-1}).

A second way to determine whether apparent proper motions are indicative of real maser motions is to compare the apparent proper motions across more than one epoch. To the extent that the apparent maser motions are real and linear, the apparent motions between epochs 1 and 2 should be equal to the apparent motions between epochs 2 and 3, with the scatter providing a measurement of the total error associated with measuring proper motions and the effects of turbulence. We select the three epochs (1) 2000 November 22 and 2001 January 6 (Fish et al. 2005), (2) 2004 September 16/19 (Fish & Reid 2007a), and (3) 2008 April 26 (this work). These epochs are roughly equally spaced in time, were all observed with several hours of on-source observing time with the same array (VLBA) and were all reduced and analysed in a similar manner. [Other epochs of VLBI data exist, such as the VLBA snapshot of Slysh et al. (2002) and the three EVN epochs of Slysh et al. (2010), but the three selected epochs have higher sensitivity (see Section 3.4).] Fig. 5 shows the correlation between proper motions from epoch 1 to 2 and from epoch 2 to 3. Excluding masers that are weaker than 0.2 Jy in an epoch (for which signal-to-noise ratio limitations in determining the centroid position in each epoch dominate) or that are spatially blended in the third epoch, the rms velocity spread in each of right ascension and declination is 1.1 km s^{-1}, with median values lower by a factor of 2. In comparison, detected proper motions are typically several times this value (Fig. 4), suggesting that the apparent proper motions are real. We also note that the velocity spread is very close to the intrinsic thermal linewidth of water masers near VLA 1 (Surcis et al. 2011) and comparable to the estimate of the turbulent velocity in OH maser cluster in W3(OH) (Reid et al. 1980), possibly indicating that turbulence is partially responsible for the observed scatter.

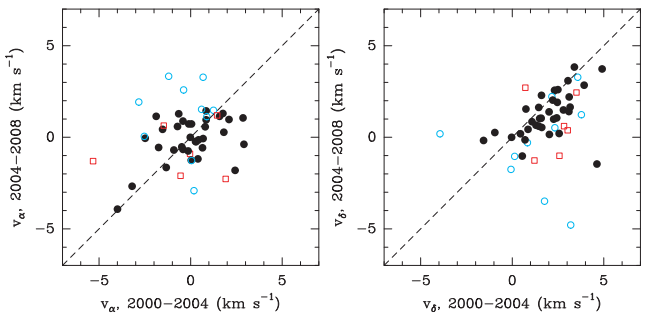

Figure 5. Comparison of apparent maser proper motions between epochs. The RA (left) and Dec. (right) component of motions between the 2004 and 2008 April epochs versus the same component between the 2000 and 2004 epochs. Spots that are spatial blends of emission from two masers in the 2008 April epoch are shown as open red squares. Open cyan circles denote masers whose minimum flux density in the three epochs is less than 0.2 Jy. Bright unblended masers are shown as filled black circles. The correlation between epochs of proper motions obtained from unblended masers indicates that the apparent proper motions are real.

A third, though less robust, estimator of the noise in apparent maser proper motions is the magnitude of the vector difference of velocities between the epochs, $|v_{23} - v_{12}|$, where the subscripts indicate epoch numbers. Neglecting weak and spatially blended masers, the median value of $|v_{23} - v_{12}|$ is 1.5 km s^{-1}. However, this estimator is not robust against random errors in determining the position of the reference feature in each epoch. For instance, a 0.5-mas error in the position of the reference feature in the third epoch could lower the median vector velocity difference to below 1.1 km s^{-1}. (In contrast, a positional error in the reference feature shifts points in the panels in Fig. 5 without affecting the scatter among the points.)

These statistics are consistent with the result of Slysh et al. (2010) that the errors in determining OH maser proper motions are significantly larger than would be estimated from the errors in determining maser centroids due solely to signal-to-noise ratio considerations (at least above a detection threshold of $\sim 20\sigma$). Nevertheless, it is also apparent that the apparent proper motions of OH masers are indeed tracing their local velocity field. Proper motion maps of OH masers can be a reliable estimator in determining motions of clusters containing multiple bright maser spots that are spatially unblended. However, caution should be exercised in interpreting small ($\lesssim$0.1 beamwidth) motions of individual masers, where systematic errors effectively introduce a large error in determining the position angle of the motion.

5 CONCLUSIONS

We detect a strong flare in the 1720-MHz OH maser emission in W75N, with the brightest RCP feature exceeding a flux density of 400 Jy. Although weak 1720-MHz masers have been detected in W75N before, the observations we report are two orders of magnitude brighter than previously observed. The 1720-MHz masers are likely produced by very dense molecular material that is excited and slowly accelerated by the outflow traced by highly variable water masers near the continuum source VLA 1. The appearance of main-line masers implying smaller magnetic fields farther down the line of the outflow supports theoretical OH maser models, which predict 1720- and 4765-MHz masers at higher densities than 1665- and 1667-MHz masers.

When compared with VLBI images of the 1665- and 1667-MHz OH masers in previous epochs, the VLBA observations reported herein are consistent with proper motions previously reported, contrary to the findings of Slysh et al. (2010). We conclude that apparent maser motions are reliable estimates of real proper motions, but note that the measurement error in determining proper motions is larger than would be expected from signal-to-noise ratio considerations alone.

ACKNOWLEDGMENTS

The National Radio Astronomy Observatory is a facility of the National Science Foundation operated under cooperative agreement by Associated Universities, Inc. MERLIN is a National Facility operated by the University of Manchester at Jodrell Bank Observatory on behalf of STFC. We thank Pierre Colom for arranging the observations at Nançay.

REFERENCES

Alakoz A. V., Slysh V. I., Popov M. V., Val'tts I. E., 2005, Astron. Lett., 31, 375

Argon A. L., Reid M. J., Menten K. M., 2000, ApJS, 129, 159
Bloemhof E. E., Reid M. J., Moran J. M., 1992, ApJ, 397, 500
Condon J. J., Cotton W. D., Greisen E. W., Yin Q. F., Perley R. A., Taylor G. B., Broderick J. J., 1998, AJ, 115, 1693
Cragg D. M., Sobolev A. M., Godfrey P. D., 2002, MNRAS, 331, 521
Crutcher R. M., 1999, ApJ, 520, 706
Davies R. D., 1974, in Kerr F. J., Simonson S. C., eds, Proc. IAU Symp. 60, Galactic Radio Astronomy. Reidel, Dordrecht, p. 275
Felli M. et al., 2007, A&A, 476, 373
Fish V. L., Reid M. J., 2007a, ApJ, 656, 952
Fish V. L., Reid M. J., 2007b, ApJ, 670, 1159
Fish V. L., Sjouwerman L. O., 2007, ApJ, 668, 331
Fish V. L., Reid M. J., Argon A. L., Zheng X.-W., 2005, ApJS, 160, 220
Fish V. L., Brisken W. F., Sjouwerman L. O., 2006, ApJ, 647, 418
Gray M. D., Field D., Doel R. C., 1992, A&A, 262, 555
Gray M. D., Hutawarakorn B., Cohen R. J., 2003, MNRAS, 343, 1067
Hunter T. R., Taylor G. B., Felli M., Tofani G., 1994, A&A, 284, 215
Hutawarakorn B., Cohen R. J., Brebner G. C., 2002, MNRAS, 330, 349
Lekht E. E., Slysh V. I., Krasnov V. V., 2009, Astron. Rep., 53, 420
Migenes V., Cohen R. J., Brebner G. C., 1992, MNRAS, 254, 501
Moellenbrock G. A., Claussen M. J., Goss W. M., 2009, ApJ, 694, 192
Niezurawska A., Szymczak M., Cohen R. J., Richards A. M. S., 2004, MNRAS, 350, 1409
Norris R. P., Booth R. S., 1981, MNRAS, 195, 213
Reid M. J., Haschick A. D., Burke B. F., Moran J. M., Johnston K. J., Swenson G. W., Jr, 1980, ApJ, 239, 89
Reid M. J., Schneps M. H., Moran J. M., Gwinn C. R., Genzel R., Downes D., Rönnäng B., 1988, ApJ, 330, 809
Richards A. M. S., Yates J. A., Cohen R. J., 1999, MNRAS, 306, 954
Rygl K. L. J. et al., 2010, 10th EVN Symposium, preprint (arXiv:1011.5042)
Slysh V. I., Migenes V., 2006, MNRAS, 369, 1497
Slysh V. I., Migenes V., Val'tts I. E., Lyubchenko S. Yu., Horiuchi S., Altunin V. I., Fomalont E. B., Inoue M., 2002, ApJ, 564, 317
Slysh V. I., Alakoz A. V., Migenes V., 2010, MNRAS, 404, 1121
Strelnitski V., Alexander J., Gezari S., Holder B. P., Moran J. M., Reid M. J., 2002, ApJ, 581, 1180
Surcis G., Vlemmings W. H. T., Curiel S., Hutawarakorn Kramer B., Torrelles J. M., Sarma A. P., 2011, A&A, 527, A48
Torrelles J. M., Gómez J. F., Rodríguez L. F., Ho P. T. P., Curiel S., Vázquez R., 1997, ApJ, 489, 744
Wright M. M., Gray M. D., Diamond P. J., 2004, MNRAS, 350, 1253

This paper has been typeset from a TEX/LATEX file prepared by the author.